
Fusing Bird View LIDAR Point Cloud and Front View Camera Image for Deep Object Detection

Zining Wang

Department of Mechanical Engineering
 University of California, Berkeley
 wangzining@berkeley.edu

Wei Zhan

Department of Mechanical Engineering
 University of California, Berkeley
 wzhan@berkeley.edu

Masayoshi Tomizuka

Department of Mechanical Engineering
 University of California, Berkeley
 tomizuka@berkeley.edu

Abstract

We propose a new method for fusing a LIDAR point cloud and camera-captured images in the deep convolutional neural network (CNN). The proposed method constructs a new layer called non-homogeneous pooling layer to transform features between bird view map and front view map. The sparse LIDAR point cloud is used to construct the mapping between the two maps. The pooling layer allows efficient fusion of the bird view and front view features at any stage of the network. This is favorable for the 3D-object detection using camera-LIDAR fusion in autonomous driving scenarios. A corresponding deep CNN is designed and tested on the KITTI[1] bird view object detection dataset, which produces 3D bounding boxes from the bird view map. The fusion method shows particular benefit for detection of pedestrians in the bird view compared to other fusion-based object detection networks.

1 Introduction

LIDAR and camera are becoming standard sensors for self-driving cars and 3D objection detection is an important part of perception in driving scenarios. 2D front view images from cameras provide rich texture descriptions of the surrounding, while depth is hard to obtain. On the other hand, 3D point cloud from LIDAR can provide accurate depth and reflection intensity information, but the resolution is comparatively low. Therefore, 2D images and 3D point cloud are supplementary to each other to accomplish accurate and robust perception. The fusion of these two sensors is a prerequisite for autonomous vehicles to deal with complicated driving scenarios.

The recent progress of convolutional neural networks (CNN) for classification and segmentation has invoked particular interest of applying deep neural networks (DNN) for object detection. The DNN-based object detection with either LIDAR [2, 3] or camera [4, 5, 6] data as the input has been widely explored by researchers and pushed to a very high single frame accuracy. However, the 3D object detection is still hard for network based on a single kind of sensor, which is shown in Table 1. The camera-based network obtains high average precision for 2D image bounding box because of the

rich texture information, which is consistent with the current CNN segmentation performance for images. Since camera does not contain accurate depth information, the 3D bounding box precision is very low for camera-based networks even with stereo vision [7] and vehicle dimension prior [4] presented. The state-of-the-art LIDAR-only networks have low precision in both 2D and 3D detection but the gap of precision between 2D and 3D detection is much lower compared to camera-only networks. This means the objects detected by LIDAR are mostly accurate in 3D location. The low precision is due to sparsity of LIDAR point cloud.

The camera and LIDAR fusion gains the capability of achieving high accuracy in both 2D and 3D detection. Some fusion-based networks [8, 9] directly adapt from the Faster-RCNN structure with proposals from LIDAR so as to preserve the 3D information. Some [10, 11] propose regions of interest from the front view but projects the LIDAR point cloud to the camera image plane for an early fusion of information. The more recent MV3D [12] designs a more complicated version of fusion after region proposal and gets the highest performance among all networks in 3D detection. All the networks to date do not fuse before region 3D proposal of interested regions, which means that the fusion only helps the classification and regression stage after highly potential objects are extracted from the 3D map. The lack of fusion in the region proposal causes recall-precision trade off, especially for pedestrians, which will be discussed in Section 4.2.

In this paper, we propose a camera and LIDAR fusion architecture in CNN that fuses features from different views in the region proposal stage. The fusion is allowed to happen before the proposal stage because it fuses the whole feature maps, which is not presented in previous fusion-based networks. The main idea is to employ LIDAR point cloud and sparse matrix multiplication to link the bird view feature map and front view feature map. A sparse non-homogeneous pooling layer is designed to transform and fuse features efficiently. A fusion-based CNN network is constructed accordingly. The representation of input is similar to the MV3D, but the fusion happens before the proposal stage. In contrast, the 3D proposal in current fusion-based networks only use the LIDAR information, while ours fuses both LIDAR and camera information for 3D proposal. Moreover, if the fusion happens only after the region proposal part, the network is forced to utilize the Faster-RCNN structure which is slow from current point of view. By letting the fusion happen in the CNN backbone, this network is able to get rid of the region "proposal subnet" + "detection subnet" structure and benefits from the speed of recently developed one-stage detection network like RetinaNet [13] and SSD [14].

Network		2D Image Bounding Box		3D Bounding Box	
Type	Name	Vehicle	Pedestrian	Vehicle	Pedestrian
Camera	Deep MANTA [4]	90.0	-	-	-
Stereo	Mono3D [7]	87.9	68.6	18.2	-
Stereo	3DOP [15]	88.6	67.5	9.5	-
LIDAR	VeloFCN [12]	70.7	-	32.1	-
LIDAR	Vote3Deep [3]	77.0	67.9	-	-
Fusion	Pose-RCNN [8]	75.8	63.4	-	-
Fusion	MV3D [12]	90.5	-	71.1	-

Table 1: 2D and 3D Detection Average Precision on KITTI dataset. Categories are of moderate difficulty.

2 Related Work

DNN for Object Detection This paragraph focuses on the recent development of DNN-based detectors that are applicable to autonomous driving scenarios. One frame captured by sensors contains multiple objects involved in driving scenarios. The DNN detector should outline variate number of objects detected in different regions of the map. As pioneered in the Selective Search methodology [16], the network slides a window or cluster dense points on the feature map to produce some regions of interest (ROIs). This is often called the region proposal stage. The ROIs are then fed to a second-stage neural network classifier to generate the class and location of the object. The first stage can be done with classic methods such as R-CNN and Fast-RCNN, or be done by another region proposal network in Faster-RCNN which improves speed compared to previous ones.

Objects in the driving scenario have various sizes in the feature map due to distances and their inherent dimensions like cars, pedestrians and cyclists. Detecting from vastly different scale is hard for the vanilla Faster-RCNN. Feature pyramid using features from multiple scales is utilized in MS-CNN [5], FPN [17] and SubCNN [18] as modification.

The above two-stage network structures are usually slow for autonomous driving with high resolution images presented. A typical Faster-RCNN takes 0.2 s for a 1080p image. More recent works start to seek for one-stage detectors to avoid the overheads caused by the extra processing between two-stages. SSD and YOLO [19] finishes classification in the proposal stage and can be much faster than two-stage detectors. The accuracy trails due to class imbalance and the most recent RetinaNet addresses the problem with focal loss [13].

Detector Based on Camera or LIDAR As the DNN for a single sensor has been developed in many other areas, their CNN backbones serve as good candidates for the separate data processing paths for fusion-based network. The most intuitive thought of extending the successful 2D CNN from images to the LIDAR point cloud is to use 3D CNN with voxel representation. Unfortunately, the computational complexity grows rapidly out of acceptable range in the large outdoor scene. The LIDAR data collected in autonomous driving scenario has its own inherent sparse property. Vote3Deep [3] conducts sparse 3D convolution to reduce computational load, but this implementation is not applied to GPU parallel acceleration. VeloFCN [2] and SqueezeSeg [20] projects point cloud to the front view with the grid according to LIDAR rotation and then applies normal 2D CNN for classification and segmentation. The front view representation of point cloud shares the same multi-scale problem as camera, because the sizes of objects change as distances vary.

The camera-based detection draws the most attention of researchers and it has been very competitive on KITTI dataset[1] with hundreds of proposed structures. Most well-performed camera-based networks including MS-CNN, RRC and modified Faster-RCNN [21] only produce high quality bounding boxes in 2D front view images. There are surprisingly some single-camera-based networks capable of 3D detection. By adding the prior part and dimension knowledge of cars and cyclists, the earlier works such as 3DVP [22] and Mono3D produces 3D bounding boxes. The more recent works such as [7] Deep3DBox [15] and DeepMANTA [4] produces even more accurate 3D boxes from monocular vision than stereo-vision-based networks such as 3DOP [23].

Fusion-Based Detector The network based on camera and LIDAR fusion, especially for pedestrian detection, has not been exploited much. Some early works [10, 11] apply early fusion by projecting LIDAR point cloud to the image plane and augment the image channels after upsampling. Such structure fuses LIDAR and camera data through the whole network but only on image plane. This means the accurate 3D information of LIDAR point cloud are almost lost in the output of the network. The position estimation banks on the regression can magically retrieve the 3D measurement of point cloud, which is not the case according to their low 3D detection precision. Pose-RCNN [8] adapts the Fast-RCNN structure where the region proposal is done by classic selective search in LIDAR voxel representation. The fusion structure does not feed LIDAR data into the deep convolutional network which means the classification relies merely on camera data. The state-of-the-art MV3D network applies region proposal network (RPN) on the point cloud projected to the bird view plane to preserve the 3D measurement in region proposal, and uses the Faster-RCNN and Deep-fused Net [24] structure to fuse LIDAR and camera data after the first stage. Note that the region proposal stage only takes in the bird view LIDAR data. The quality of the proposals is limited by the single view and single sensor information. The speed is also limited as the fusion must happen at the second stage. In this paper, we propose an efficient fusion scheme in the first stage. The proposal takes into account the information from both CNN-processed bird view LIDAR and front view camera. This structures produces high quality proposals by camera and LIDAR fusion and allows building one-stage fusion-based detectors.

3 Sparse Non-homogeneous Pooling with LIDAR Point Cloud

The sparse non-homogeneous pooling is a method that transforms two feature maps $f(x, y), g(u, v)$, where the transformation is linear but non-homogeneous. For example, the general convolution and

pooling used in CNNs are homogeneous since

$$f(x, y) = \sum_{u, v} k(x - u, y - v) g(u, v)$$

where the kernel $k(u, v)$ has the same finite support on (u, v) , such as $[-1, 1] \times [-1, 1]$ with the kernel size of 3, which is independent of (x, y) . The spatial transformer network [25] is also homogeneous as it predicts a uniform transformation matrix for the whole feature map. In general, the camera image map and bird view map is related by the projective transformation

$$\begin{bmatrix} uw \\ vw \\ w \end{bmatrix} = P \begin{bmatrix} x \\ y \\ z \\ 1 \end{bmatrix}$$

where P is the projection matrix derived from camera-LIDAR calibration, (u, v) is the pixel in image and (x, y) is the coordinate in bird view map. z is the additional height coordinate. If we want to transform a feature map from image to bird view, the transformation is

$$f(x, y) = \sum_{u, v} k_{x, y}(u, v) g(u, v)$$

and the support of kernel is $\sup(k_{x, y}) = \left\{ (u, v) \mid [u, v]^T = w^{-1} P_{12} X, w \in \mathbb{R}^+ \right\}$ where $X = [x, y, z, 1]^T$ and P_{12} constains the first two rows of P . Both the elements and measure of the support depends on (x, y) . The support is usually a line. If the transformation was done as above, the computation would be heavy and non-parallel because a large but various number of $g(u, v)$'s was involved for each (x, y) . The sparse non-homogeneous pooling uses the LIDAR point cloud to reduce the support region. It also formulates the transformation as sparse matrix multiplication so that pooling of the full future map is done in one matrix multiplication.

3.1 Bird View LIDAR representation

The most important coordinate information of 3D object detection in autonomous driving scenarios is the x, y and orientation on the ground. In fact, height can be easily estimated from the ground. Bird view takes the ground plane for the feature map and thus provides the best proposal on x, y axis which are more difficult to estimate. Currently, no front view detector has achieved good performance on the 3D bounding box proposal. In bird view representation, point cloud is discretized into a $L_b \times W_b \times H_b$ grid. The $L_b \times W_b$ grid on the ground is dense and H_b is small so that the number of cells is similar to a 2D grid instead of 3D voxel representation. Each cell encodes the density of points inside. The density is normalized by the distance-density curve so that the density is uniform for far and nearby objects.

3.2 Non-homogeneous Pooling as Sparse Matrix Multiplication

The transformation between front view (image) map and bird view map can be sparsified by the LIDAR point cloud. In stead of one pixel (u, v) in front view corresponds to a full homogeneous line $(\lambda x, \lambda y)$ in bird view, only the (u, v) and (x, y) that shares the same point in LIDAR point cloud are paired. The transformation is still non-homogeneous as the pairing does not guarantee one-to-n (n fixed) mapping, but the computation is sparse as the number of points in point cloud is of only 10,000 scale. Suppose the front view map is of size $H_f \times W_f$ and the bird view map is $L_b \times W_b$. The LIDAR point cloud is $\{(x_i, y_i, z_i) \mid i = 1, 2, \dots, N\}$, the transformation kernel is sparsified as

$$k_{x, y}(u, v) = \delta_{(x, y)(x_i, y_i)} k_{x, y}(u, v) \delta_{(u, v)(u_j, v_j)}, \quad i, j = 1, 2, \dots, N$$

because only $(u, v), (x, y)$ correspond to a point of LIDAR point cloud are transformed. The transformation becomes

$$\begin{aligned} f(x_i, y_i) &= \sum_{u, v} k_{x_i, y_i}(u, v) \delta_{(u, v)(u_j, v_j)} g(u, v) \\ &= \sum_j k_{x_i, y_i}(u_j, v_j) g(u_j, v_j) \\ &= \sum_j k_{x_i, y_i}(u_j, v_j) \delta_{(x_i, y_i)(x_j, y_j)} g(u_j, v_j) \end{aligned}$$

where

$$\delta_{ab} = \begin{cases} 1, & a = b \\ 0, & \text{otherwise} \end{cases}$$

So the transformation kernel, instead of having a small support like convolution, is a sparse $L_b W_b \times H_f W_f$ matrix of $\{(x, y)\} \times \{(u, v)\}$, or of $\mathbb{Z}_N / \sim \times \mathbb{Z}_N$ where \sim is the equality

$$(x_i, y_i) \sim (x_j, y_j) \Leftrightarrow (x_i, y_i) = (x_j, y_j)$$

There are at most N non-zero elements in the sparse matrix regardless of the size of feature maps. This one is the nearest neighbor pooling so the kernel is $k = 1$. Note this can be extend to more general interpolation method like bilinear pooling by associating the LIDAR point cloud with not only the one pixel it projects to but also its neighbors and normalize the matrix row-wise to have sum 1.

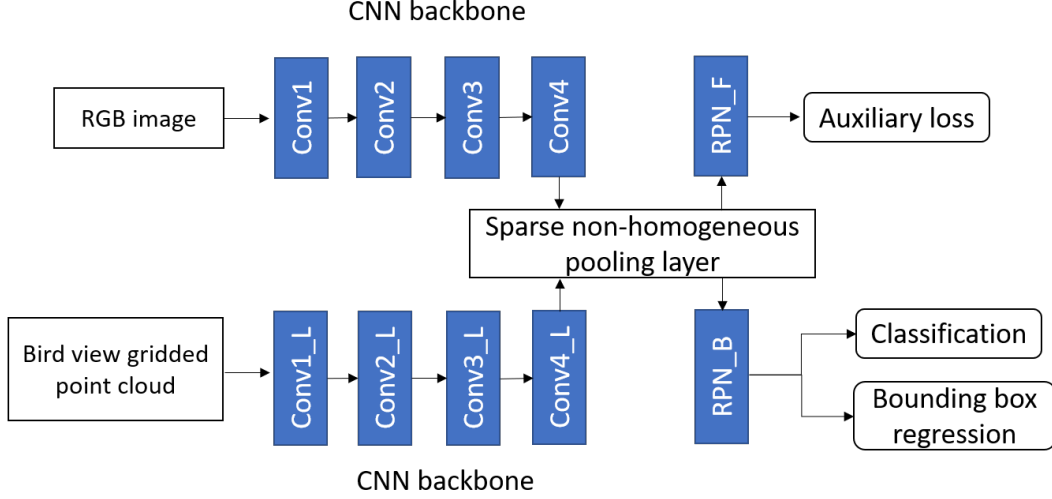


Figure 1: The fusion-based one-stage object detection network.

3.3 Fusion of Front View and Bird View Features

Section 3.2 introduces the case of transformation from front view (u, v) to bird view (x, y) but this can also be done from bird view to front view by just exchanging the coordinates. When applying the non-homogeneous pooling in network, since all the coordinate of the feature maps and the calibration matrix P are known, the pairs and matrix can be pre-calculated for each frame. There is no parameter to train for the pooling operation. The structure of the layer is illustrated in Figure 2

The sparse non-homogeneous pooling layer takes the feature map, such as the image, as input and $(u_i, v_i), (x_i, y_i)$ pairs as parameters. The kernel value is an optional input that can be specified, otherwise set as default 1. The layer constructs a $L_b W_b \times H_f W_f$ sparse matrix M . The $H_f \times W_f \times C$ feature map is flatten to a dense $H_f W_f \times C$ matrix F . Then the pulled feature map is $B = MF$ of $L_b W_b \times C$ and can be concatenated with the target feature map for further processing. Batch normalization (BN) is applied for both feature before right before concatenation.

The fusion between bird view and front view feature by using the nearest neighbor pooling is not recommended in the early stage. Due to the low resolution of LIDAR point cloud compared to the camera image, pooling of raw input results in a very low usage of image data shown in Figure 3. 20,000 point cloud only results in 0.4% usage of pixels in raw RGB image in KITTI dataset. The sparse pooling is preferred to be applied to deeper layers like the network shown in Figure 1. When the pooling is done at the conv4 layer where the raw input has been downsampled by 8, most of the front view and bird view features are involved in fusion except for the part of sky or out of the range of view.

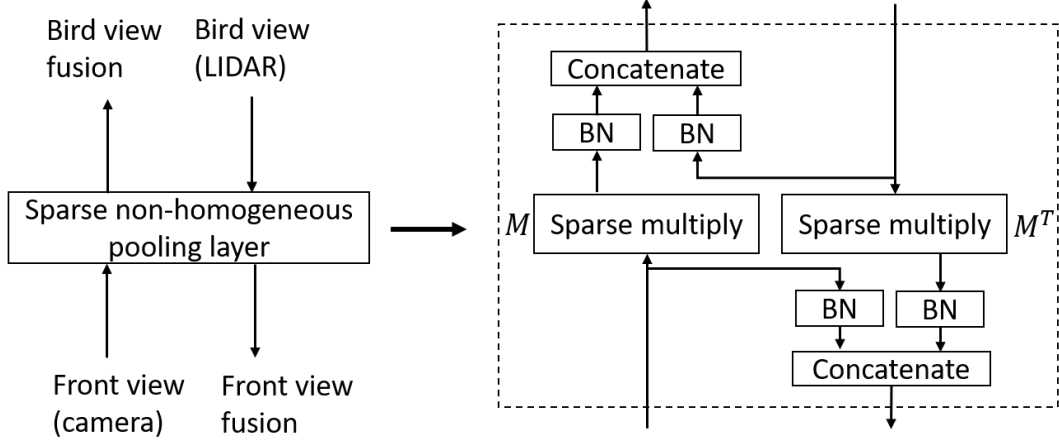


Figure 2: The sparse non-homogeneous pooling layer that fuses front view image and bird view LIDAR feature.

4 One-Stage Fusion-Based Detection Network

The fusion structure introduced in Section 3 allows one-stage detector because the fusion is done in the first stage across different view, unlike [12] where fusion is done only after RoI pooling in the second stage. In this section we introduce a one-stage detection that takes front view camera image and bird view LIDAR point cloud as input and produces 3D bounding box from bird view without RoI pooling. The detection scheme is adapted from [13] but those of [14, 19] are also compatible.

4.1 3D Region Proposal with Fusion structure

The network structure is shown in Figure 1. There are two fully convolutional backbones, namely the image CNN and LIDAR CNN. The sparse non-homogeneous pooling layer serves as the cross-bridge of two path to exchange information from each sensor. The image CNN adapts the similar RPN structure recent camera-based one-stage detections. Although the region proposal is not used during test, a separate loss is imposed on the image CNN so that image features get supervision from the label in front view in addition to the that from the 3D proposal.

Since the region proposal is in the bird view, object of different distances are of the similar size if they are in the same category. The vehicles in KITTI dataset have bounding box size (l, w, h) of $(4.0, 1.6, 1.6)m \pm (0.6, 0.1, 0.2)m$ and pedestrians are of $(0.9, 0.6, 1.6)m \pm (0.2, 0.1, 0.2)m$ in the bird view plane. There is no multi-scale issue as in the front view plane hence the multi-scale structure in [12, 17] are not needed.

4.2 One-Stage Object Detection

The resolution of image and bird view point cloud being processed in autonomous driving scenario is much larger than the benchmark datasets used to evaluate general detection networks. The test time per frame is important for practical application. One-stage detector is much faster than the two-stage detectors because it does not have the RoI pooling, non-minimum suppression and fully connected operation in the second stage. One-stage detector directly predict bounding boxes from all the proposals produced by RPN which is usually of 100K scale which means the proposals should be of very high quality to extract the very few true positives.

Class Imbalance and Hard Negative Mining The class imbalance problem in detectors based on selective search [16] and its solution in DNNs is summarized in [13]. For two-stage detectors [26], the imbalance problem is addressed by RoI pooling as the RoI pooled keeps a positive:negative $\approx 1:3$ in the second stage. Actually other second stage detectors like [12] also uses bootstrapping and weighted class loss in the first stage when the class imbalance is huge for small objects.

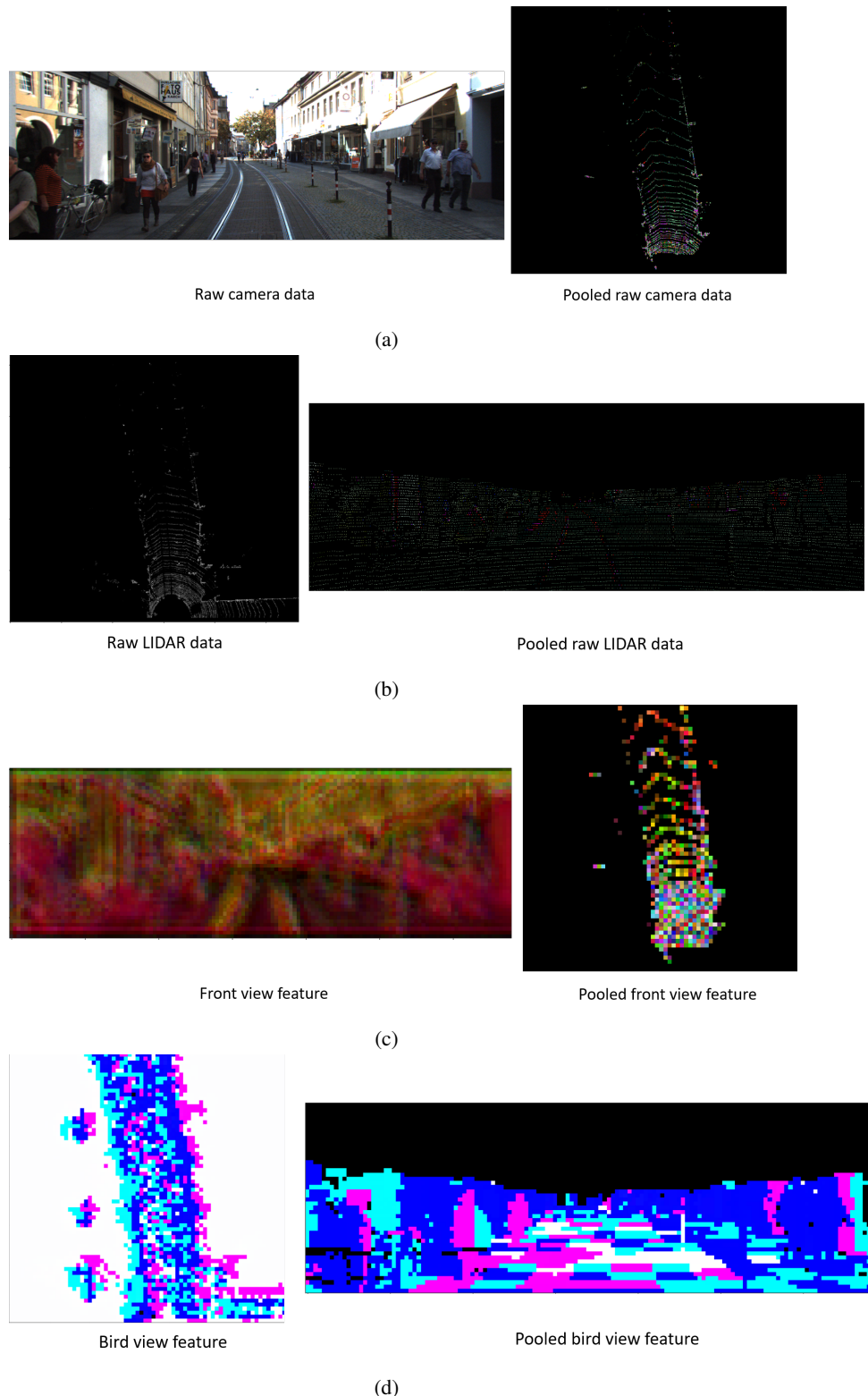


Figure 3: The sparse non-homogeneous pooling example: (a)From camera image to bird view. (b)From bird view to camera image. (c)From front view conv4 layer to bird view conv4 layer. (d)From bird view conv4 to bird view conv4.

Class imbalance problem is because in addition to the prediction of probability, classification also in effect a binary (or discrete) decision [27]. A utility function or decision cost is imposed to the classification result where true negatives whose probability is below some threshold contribution no cost. The so called hard negative mining solutions share the same idea of lifting the loss of hard negatives which have high predicted object probability, because there is a mismatch between the cross-entropy loss and decision loss. This work uses the focal loss [13] which is a weighted sum of cross-entropy

$$\text{FL}(\mathbf{p}, y) = \alpha_y (1 - p_y)^\gamma \text{CE}(\mathbf{p}, y)$$

where \mathbf{p} is the vector of probability of the sample among all classes. y is the label of the sample. $p_y = \mathbf{p}(y)$ is the probability at class y and α_y is an empirical weight for each class. $\text{CE}(\cdot)$ is the cross-entropy. It is very efficient and demonstrated to be effective on image-based one-stage object detector by [13].

Pedestrian Labeling in Bird View Map MV3D is very successful on the 3D detection of vehicles by outperforming all other methods on KITTI by a large margin. However, it does not have detection score on the pedestrian and cyclist class. On the one hand the reason is because vehicles have very distinguishable feature on the bird view map as square corners but pedestrians are only dense dots similar to trees and traffic signs. On the other hand, The size of pedestrian on the bird view map where region proposals come from are very small. The general size of pedestrian is $1m \times 0.6m$ which is only 10×6 with a resolution of $0.1m$ on a 600×600 bird view representation. Even with a down-sample rate of 4, its anchor becomes 2.5×1.5 . One shift will cause the IoU (interaction over union) fall off 0.5. In practice, it is observed that the maximum IoU between anchors and ground truth box is usually less than 0.5 for pedestrians. This is the general labeling method in detection networks which is by IoU>0.5 between anchor and ground truth box is not suitable for pedestrians.

5 Experiments

The network based on sparse non-homogeneous pooling is evaluated on the KITTI dataset which has calibrated camera and LIDAR data and ground truth 3D bounding boxes. The KITTI 3D object and bird view evaluation is used. We focus on the pedestrian category as the maximum average precision (mAP) on KITTI is still very low for all the existing methods where average precision (AP) is only about 26%. It is shown that the fusion structure helps a lot for the 3D proposal of pedestrians from bird view since there is enough fused information.

5.1 Implementation

Network Details Two kinds of CNN backbone are used for the network, namely the widely use VGG16 and ResNet. The VGG16 is full VGG pretrained on ImageNet in contrast to the reduced VGG used in [12]. The network is implemented using TensorFlow and one TITAN X GPU as hardware. The input is the 1242×375 camera image and the $600 \times 600 \times 9$ gridded LIDAR bird view representation with $0.1m$ resolution on the ground. The inputs are augmented by random shifting and calibration matrix for pooling is changed accordingly. The feature map produced by the backbone is down-sampled by 8 times but up-sampled by 2 through deconv layer before region proposal.

The focal loss is applied to the all anchors to deal with the class imbalance. Different from [13], it is observed that using the focal loss for the non-object class only and cross-entropy for object classes performs better than using focal loss for all classes. The same smooth l_1 loss [28] is used for bounding box regression.

Evaluation Speed The sparse non-homogeneous pooling layer is tested to be efficient. The pooling of raw inputs (camera image and bird view LIDAR above) takes 20ms while the pooling of features produced by VGG16 ($155 \times 46 \times 512$ for camera and $75 \times 75 \times 512$ for LIDAR) takes 14ms. With the efficient sparse non-homogeneous pooling fusion and one-stage detection structure, the test time is 0.11s per frame compared to the 0.7s per frame in MV3D. The test time is consist of the sparse matrix construction, network forward and bounding box post-processing (NMS) but the file I/O is excluded.

The network is trained on the KITTI object detection benchmark using the same train/validation split as provided in [5]. The bird view average precision is used for evaluation. Actually the AP on bird view benchmark is very similar to the 3D benchmark of KITTI for all methods involved.

5.2 Quality of Proposals

To verify the fusion structure is helping augmenting the feature in the RPN, the recall and precision in the RPN with VGG16 is compared with that of the MV3D structure. To make fair comparison, the cross-entropy loss is used in RPN instead of focal loss and IoU threshold is set to 0.5. The MV3D implemented in this paper is unofficial but reproduced according to the paper. Table 2 shows for vehicles, the precisions are similar but for pedestrians, the fusion-based RPN has much higher precision. This is because the pedestrian is hard to distinguish with other obstacles by just bird view LIDAR data, while vehicles are distinct from bird view. The proposals for pedestrians requires more information and the fusion structure provides the front view image feature which makes proposal quality of pedestrians similar to that of vehicles.

Network	Vehicle		Pedestrian		
	Type	Recall	Precision	Recall	Precision
MV3D	99.4	17.3	97.8	4.2	
ours	99.2	19.5	96.6	17.3	

Table 2: RPN performance of RPN on pedestrian and vehicles on the validation set. All difficulty levels are included

5.3 Detection Results and Discussion

The pedestrian detection result is evaluated on the validation dataset and shown in Figure 4. There is a large overfitting between the training set and validation set which requires further tuning.

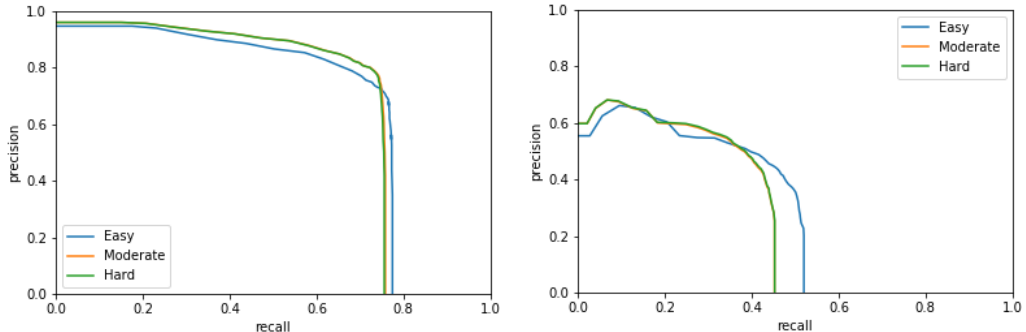


Figure 4: The PR-curve on training and validation set.

Network	Pedestrian			
	Name	Easy	Moderate	Hard
3dssd	27.4	24.0	22.4	
AVOD	34.4	26.1	24.2	
ours	32.0	29.4	29.3	

Table 3: Comparison with the current state of the art on KITTI. Note our AP is on the validation set and other APs are on the test set. Both the state of the art are anonymous.

6 Conclusion

We have proposed a sparse non-homogeneous pooling method to efficiently transform and fuse features from different views. The fusion is allowed to happen before the proposal stage because it fuses the whole feature map, which is not presented in previous fusion-based networks. The corresponding one stage detector designed produces high quality 3D proposals. The detector achieves good performance in the 3D detections of pedestrians from bird view on KITTI dataset where the state of art detectors performs poorly.

References

- [1] Andreas Geiger, Philip Lenz, and Raquel Urtasun. Are we ready for autonomous driving? the kitti vision benchmark suite. In *Computer Vision and Pattern Recognition (CVPR), 2012 IEEE Conference on*, pages 3354–3361. IEEE, 2012.
- [2] Bo Li, Tianlei Zhang, and Tian Xia. Vehicle detection from 3d lidar using fully convolutional network. *arXiv preprint arXiv:1608.07916*, 2016.
- [3] Martin Engelcke, Dushyant Rao, Dominic Zeng Wang, Chi Hay Tong, and Ingmar Posner. Vote3deep: Fast object detection in 3d point clouds using efficient convolutional neural networks. In *Robotics and Automation (ICRA), 2017 IEEE International Conference*, pages 1355–1361. IEEE, 2017.
- [4] Florian Chabot, Mohamed Chaouch, Jaonary Rabarisoa, Céline Teuli  re, and Thierry Chateau. Deep manta: A coarse-to-fine many-task network for joint 2d and 3d vehicle analysis from monocular image. *arXiv preprint arXiv:1703.07570*, 2017.
- [5] Zhaowei Cai, Quanfu Fan, Rogerio S Feris, and Nuno Vasconcelos. A unified multi-scale deep convolutional neural network for fast object detection. In *European Conference on Computer Vision*, pages 354–370. Springer, 2016.
- [6] Jimmy Ren, Xiaohao Chen, Jianbo Liu, Wenxiu Sun, Jiahao Pang, Qiong Yan, Yu-Wing Tai, and Li Xu. Accurate single stage detector using recurrent rolling convolution. *arXiv preprint arXiv:1704.05776*, 2017.
- [7] Xiaozhi Chen, Kaustav Kundu, Ziyu Zhang, Huimin Ma, Sanja Fidler, and Raquel Urtasun. Monocular 3d object detection for autonomous driving. In *Proceedings of the IEEE Conference on Computer Vision and Pattern Recognition*, pages 2147–2156, 2016.
- [8] Markus Braun, Qing Rao, Yikang Wang, and Fabian Flohr. Pose-rcnn: Joint object detection and pose estimation using 3d object proposals. In *Intelligent Transportation Systems (ITSC), 2016 IEEE 19th International Conference on*, pages 1546–1551. IEEE, 2016.
- [9] Alireza Asvadi, Lu  s Garrote, Cristiano Premebida, Paulo Peixoto, and Urbano Nunes. Depthen: Vehicle detection using 3d-lidar and convnet. In *Intelligent Transportation Systems (ITSC), IEEE 20th International Conference*. IEEE, 2017.
- [10] Taewan Kim and Joydeep Ghosh. Robust detection of non-motorized road users using deep learning on optical and lidar data. In *Intelligent Transportation Systems (ITSC), 2016 IEEE 19th International Conference on*, pages 271–276. IEEE, 2016.
- [11] Stefan Lange, Fritz Ulbrich, and Daniel Goehring. Online vehicle detection using deep neural networks and lidar based preselected image patches. In *Intelligent Vehicles Symposium (IV), 2016 IEEE*, pages 954–959. IEEE, 2016.
- [12] Xiaozhi Chen, Huimin Ma, Ji Wan, Bo Li, and Tian Xia. Multi-view 3d object detection network for autonomous driving. *arXiv preprint arXiv:1611.07759*, 2016.
- [13] Tsung-Yi Lin, Priya Goyal, Ross Girshick, Kaiming He, and Piotr Doll  r. Focal loss for dense object detection. *arXiv preprint arXiv:1708.02002*, 2017.
- [14] Wei Liu, Dragomir Anguelov, Dumitru Erhan, Christian Szegedy, Scott Reed, Cheng-Yang Fu, and Alexander C Berg. Ssd: Single shot multibox detector. In *European conference on computer vision*, pages 21–37. Springer, 2016.
- [15] Arsalan Mousavian, Dragomir Anguelov, John Flynn, and Jana Kosecka. 3d bounding box estimation using deep learning and geometry. *arXiv preprint arXiv:1612.00496*, 2016.

- [16] Jasper RR Uijlings, Koen EA Van De Sande, Theo Gevers, and Arnold WM Smeulders. Selective search for object recognition. *International journal of computer vision*, 104(2):154–171, 2013.
- [17] Tsung-Yi Lin, Piotr Dollár, Ross Girshick, Kaiming He, Bharath Hariharan, and Serge Belongie. Feature pyramid networks for object detection. *arXiv preprint arXiv:1612.03144*, 2016.
- [18] Yu Xiang, Wongun Choi, Yuanqing Lin, and Silvio Savarese. Subcategory-aware convolutional neural networks for object proposals and detection. In *Applications of Computer Vision (WACV), 2017 IEEE Winter Conference on*, pages 924–933. IEEE, 2017.
- [19] Joseph Redmon and Ali Farhadi. Yolo9000: better, faster, stronger. *arXiv preprint arXiv:1612.08242*, 2016.
- [20] Bichen Wu, Alvin Wan, Xiangyu Yue, and Kurt Keutzer. Squeezeseg: Convolutional neural nets with recurrent crf for real-time road-object segmentation from 3d lidar point cloud. *arXiv preprint arXiv:1710.07368*, 2017.
- [21] Fan Yang, Wongun Choi, and Yuanqing Lin. Exploit all the layers: Fast and accurate cnn object detector with scale dependent pooling and cascaded rejection classifiers. In *Proceedings of the IEEE Conference on Computer Vision and Pattern Recognition*, pages 2129–2137, 2016.
- [22] Yu Xiang, Wongun Choi, Yuanqing Lin, and Silvio Savarese. Data-driven 3d voxel patterns for object category recognition. In *Proceedings of the IEEE Conference on Computer Vision and Pattern Recognition*, pages 1903–1911, 2015.
- [23] Xiaozhi Chen, Kaustav Kundu, Yukun Zhu, Andrew G Berneshawi, Huimin Ma, Sanja Fidler, and Raquel Urtasun. 3d object proposals for accurate object class detection. In *Advances in Neural Information Processing Systems*, pages 424–432, 2015.
- [24] Jingdong Wang, Zhen Wei, Ting Zhang, and Wenjun Zeng. Deeply-fused nets. *arXiv preprint arXiv:1605.07716*, 2016.
- [25] Max Jaderberg, Karen Simonyan, Andrew Zisserman, et al. Spatial transformer networks. In *Advances in Neural Information Processing Systems*, pages 2017–2025, 2015.
- [26] Shaoqing Ren, Kaiming He, Ross Girshick, and Jian Sun. Faster r-cnn: Towards real-time object detection with region proposal networks. In *Advances in neural information processing systems*, pages 91–99, 2015.
- [27] Frank E Harrell Jr. *Regression modeling strategies: with applications to linear models, logistic and ordinal regression, and survival analysis*, chapter Prediction vs. Classification, pages 4–5. Springer, 2015.
- [28] Ross Girshick. Fast r-cnn. In *Proceedings of the IEEE international conference on computer vision*, pages 1440–1448, 2015.